Biogeosciences
Discussions

Open Access

Enhanced pH up-regulation enables the cold-water coral *Lophelia pertusa* to sustain growth in aragonite undersaturated conditions

M. Wall[1,2], F. Ragazzola[3,*], L. C. Foster[3,**], A. Form[1], and D. N. Schmidt[3]

[1]GEOMAR Helmholtz Centre for Ocean Research Kiel, Germany
[2]Alfred Wegener Institute for Polar and Marine Research, Bremerhaven, Germany
[3]School of Earth Sciences, University of Bristol, UK
[*]now at: Institute of Marine Sciences, Portsmouth University, UK
[**]now at: Marine conservation society, Unit 3, Hereford and Worcester, UK

Correspondence to: M. Wall (mwall@geomar.de)

BGD

12, 6757–6781, 2015

Enhanced pH up-regulation enables the cold-water coral *Lophelia pertusa*

M. Wall et al.

Title Page

Abstract	Introduction
Conclusions	References
Tables	Figures

◄◄ ►►

◄ ►

Back Close

Full Screen / Esc

Printer-friendly Version

Interactive Discussion

Abstract

Cold-water corals are important habitat formers in deep-water ecosystems and at high latitudes. Ocean acidification and the resulting change in aragonite saturation are expected to affect these habitats and impact coral growth. Counter to expectations, the
5 impact of saturation changes on the deep water coral *Lophelia pertusa* has been found to be less than expected, with the species sustaining growth even in undersaturated conditions. However, it is important to know whether such acclimation modifies the skeleton and thus its ecosystem functioning. Here we used Synchrotron X-Ray Tomography and Raman spectroscopy to examine changes in skeleton morphology and
10 fibre orientation. We combined the morphological assessment with boron isotope analysis to determine if changes in growth are related to changes in control of calcification pH. Skeletal morphology is highly variable without clear changes in different saturation states. Raman investigations found no difference in macromorphological skeletal arrangement of early mineralization zones and secondary thickening between the treat-
15 ments but revealed that the skeletal organic matrix layers were less distinct. The δ^{11}B analyses show that *L. pertusa* up-regulates the internal calcifying fluid pH (pH_{cf}) during calcification with disregard to ambient seawater pH and suggests that well-fed individuals can sustain a high internal pH_{cf}. This indicates that any extra energetic demand required for calcification at low saturation is not detrimental to the skeletal morphology.

1   Introduction

The ocean is absorbing CO_2 from anthropogenic emissions resulting in a drop in carbonate saturation and ocean pH (Bates et al., 2012). Cold waters take up and store more CO_2 and thus the high latitudes will be amongst the first to experience undersaturated conditions (Orr et al., 2005a). The response of marine calcifiers to ocean acid-
25 ification has been shown to be taxon specific (Doney et al., 2009; Ries et al., 2009), so understanding the response of important key marine habitat builders is impera-

tive to estimate impacts on their future ecosystem service. While some species have been shown to continue to grow even under low pH conditions, a weakening of the ultra-structure can occur and impair ecosystem functionality i.e. its ability to withstand predator and wave action (Chan et al., 2012; Ragazzola et al., 2012).

Cold-water corals are important habitat builders that offer a range of microhabitats sustaining high biodiversity. Moreover, cold-water corals provide nursery grounds for various species of fish (Fosså et al., 2002; Henry and Roberts, 2007; Roberts et al., 2008) and thus the maintenance of their structural integrity is highly essential for a wide range of species which depend on this ecosystem. *Lophelia pertusa* is the most common species of cold-water corals and has a cosmopolitan distribution with a wide temperature (4–12 °C) and salinity range (35–37 psu) suggesting a relatively high-tolerance to environmental drivers. They are typically found in regions with strong water currents and high productivity (Genin et al., 1986; Mienis et al., 2007). The modern distribution of cold-water corals appears to be constrained by the aragonite saturation horizon (the depth below which the waters become undersaturated with respect to aragonite), with 95 % of all cold-water coral reefs found above the aragonite saturation horizon (Davies and Guinotte, 2011; Guinotte and Fabry, 2008). The aragonite saturation horizon has shoaled by 80–400 m in the North Atlantic (Feely et al., 2004) since the industrial revolution and model projections suggest a shoaling of up to 2000 m by the end of this century (Orr et al., 2005b).

Lophelia pertusa can calcify in undersaturated conditions (Form and Riebesell, 2012; Hennige et al., 2014; Maier et al., 2009, 2012) likely facilitated by its ability to increase the internal calcifying fluid pH at the site of calcification (pH_{cf}), termed "up-regulation". Most indications for up-regulation come from indirect determinations, e.g. measuring the boron isotopic composition ($\delta^{11}B$) of bulk skeleton samples of corals (Anagnostou et al., 2012; Holcomb et al., 2014; McCulloch et al., 2012; Trotter et al., 2011). Measurement of the pH_{cf} at the site of calcifications in several corals confirmed an ability of the organism to influence the pH_{cf} (Al-Horani, 2003; Ries, 2011; Venn et al., 2013). The skeletal $\delta^{11}B$ was observed to decrease with lower saturation state and pH of seawater

(pH_{sw}), suggesting lower internal pH_{cf}. At low seawater pH_{sw}, internal pH_{cf} is elevated compared to seawater pH (up-regulation intensity, where $\Delta pH = pH_{cf} - pH_{sw}$, Anagnostou et al., 2012; McCulloch et al., 2012; Trotter et al., 2011), but does not reach internal pH_{cf} levels observed under control conditions (Holcomb et al., 2014; Trotter et al., 2011).

This up-regulation ability has several implications: firstly, the potential to moderate the impact of projected future saturation state depends on the strength and efficiency to up-regulate pH (less efficient up-regulating species may be more adversely affected). In turn, such differences in efficiencies will affect $\delta^{11}B$ as pH proxy which must be considered in paleo-climate reconstruction. Secondly, the establishment of a pH gradient between external seawater and internal site of calcification requires energy (Al-Horani et al., 2003; Chalker and Taylor, 1975) and altered energetic demands may effect skeletal structure and strength.

In order to understand the interaction of biomineralisation response, up-regulation and pH_{sw} we analysed *L. pertusa* skeletons grown under natural control (Sula Reef pCO_2 = 405 µatm), moderate (CRSI pCO_2 = 604 µatm) and elevated CO_2 conditions (CRSII pCO_2 = 778 µatm, CRSIII pCO_2 = 982 µatm). Form and Riebesell (2012) provide more details about the experimental set-up (treatment conditions are summarized also in Table S1 in the Supplement). We uniquely combined Raman spectroscopy, Secondary Ionisation Mass Spectrometry (SIMS) and Synchrotron X-ray Tomographic Microscopy (SXRTM) to examine whether ocean acidification causes any change in skeletal morphology of *L. pertusa*, such as thickness and growth patterns, or in the biomineralisation processes. SIMS $\delta^{11}B$ transects are compared between the high pCO_2 (CRSIII) treatment, the natural conditions (Sula Reef) as well as different skeletal regions. The $\delta^{11}B$ are converted to pH_{cf} to examine potential physiological adjustments in coral biomineralisation under anticipated future ocean conditions of lower pH.

2 Material and methods

2.1 Specimens

Lophelia pertusa specimens came from the experimental set-up at GEOMAR, Germany. Specimens from different CO_2 levels were analyzed. The live branches of *L. pertusa* were collected with minimal invasion using the manned submersible JAGO at the central part of the Sula Reef complex (64°06′ N, 8°05′ E) off the Norwegian coast in 2008. The samples were transferred to Kiel and after a 3 month acclimatisation period they were stained using Alizarin Red S (Standard Fluka: Sigma-Aldrich, Steinheim, Germany, with a concentration of $5\,\mathrm{mg\,L^{-1}}$ for an incubation period of eight days to mark the commencement of the experiment). The corals were kept at a constant temperature (7.5 °C) and salinity (34.5) similar to their native origin at the Sula Reef (see Table S1; full details of the culturing method are described in Form and Riebesell (2012). After staining, the corals were transferred to the treatment tanks and the $p\mathrm{CO_2}$ was gradually over two weeks adjusted to the treatment conditions.

For Raman and SIMS analyses, specimens cultured in the extreme treatment ($982 \pm 146\,\mu\mathrm{atm}$) were compared to colony branches grown naturally in the field. The specimens were cut transversal (at different heights along the corallite) and longitudinal. One specimen from the high $p\mathrm{CO_2}$ treatment (CRSIII) was cut above and below the Alizarin stain (Fig. 1b). The sample preparations allow a comparison of skeleton grown naturally in situ to pre-study conditions and during the culturing time prior to the staining as well as the treatment conditions after staining.

2.2 Synchrotron analyses

Synchrotron-based X-ray Tomographic Microscopy were performed at the TOMCAT beamline at the Swiss Light Source, Paul Scherrer Institut, Villigen, Switzerland (Stampanoni et al., 2006). One specimen from each of the CO_2 levels was scanned (CRSI-CRSIII: 604 ± 105, 778 ± 112 and $982 \pm 146\,\mu\mathrm{atm}$). For each tomographic scan, 377

projections over 180° were acquired at energy of 28 keV with UPLAPO 2× objective (field view of 7.5 mm × 7.5 mm; pixel size 3.7 mm × 3.7 mm). The exposure time was 250 ms. Further processing was done using Avizo to produce 3-D isosurface model and measure sample thickness above and below Alizarin stain by cross-referencing to the sample (Fig. 1a and b).

2.3 Raman mapping

Raman mapping was done using a WITec alpha 300 R (WITec GmbH, Germany) Confocal Raman Microscope equipped with an ultra high throughput spectrometer (UHTS 300, WITec, Germany) and an EMCCD camera (grating of 600 grooves mm^{-1}, blazed at 500 nm and centred at 2400 cm^{-1}). Laser excitation wavelength of 488 nm was used. Raman maps were derived using a Nikon 20× (numeric aperture (NA) = 0.4) objective for large area scans and a Nikon 100× (NA = 0.9) for small high-resolution area scans. The spectra during mapping were recorded with an integration time of 35 ms and a step size of 1 μm (large area scans) and 10 ms and 0.5 μm for small area scans. The symmetric stretch of the carbonate (1085 cm^{-1}) provides information on the crystal orientations and was used to map the skeletal growth patterns and arrangement. Fluorescence intensity distribution (in the spectral range between 2400–2700 cm^{-1}) was used as a proxy to map organic matrix distribution within biogenic minerals (Wall and Nehrke, 2012) as well as to map the location of the staining line where it was not visible in microscopic images. All Raman spectral data sets were processed using the WITec Project software (version 2.04, WITec GmbH, Germany).

Transversal sections of *L. pertusa* calices show differences in skeletal densities (Fig. 2a) visible as differences in opaqueness of the skeleton. This criterion is often used to determine growth rings and to identify nucleation zones, which are characterized by distinct elemental ratios and isotopic signatures (Mortensen and Rapp, 1998; Wainright, 1964) compared to the bulk thecal skeleton (Adkins et al., 2003; Blamart et al., 2007; Cohen et al., 2006). Confocal Raman maps of the aragonite symmetric stretch intensity (the intensity of the main carbonate peak) allows similarly to distin-

guish the different skeletal regions (for detailed information see Wall and Nehrke, 2012). Here, skeletal regions were divided into a primary skeleton around the central corallite line (composed of EMZ) and paralleled layered fibre growth, giving the corallites their shape and size. A secondary thickening is subsequently responsible for the addition of skeletal mass to the corallite theca (Fig. 2e). The growth patterns within primary and secondary skeleton are compared between natural conditions and the treatments and used to relate the boron isotopic signature to the different growth stages.

2.4 δ^{11}B with SIMS

Boron isotopes in marine biogenic carbonates are a pH-proxy, that vary systematically with seawater pH (Anagnostou et al., 2012; McCulloch et al., 2012; Trotter et al., 2011). The value recorded depends on a strong biological control ("vital effect") and reflects internal calcifying fluid pH_{cf} (Holcomb et al., 2014; McCulloch et al., 2012). The following equation converts δ^{11}B into pH (or pH_{cf}):

$$pH = pK_B^* - \log\left[\frac{\delta^{11}B_{sw} - \delta^{11}B_C}{\alpha_B \times \delta^{11}B_C - \delta^{11}B_{sw} + 1000 \times (\alpha_B - 1)}\right] \qquad (1)$$

pK_B^* = dissociation constant of boric acid (Dickson, 1990). The theoretical δ^{11}B for the sample location can be calculated using pK_B^* = 8.795 for the natural in situ grown skeletal and pK_B^* = 8.814 for the treatment corals. pK_B^* values were calculated from seacarb using the software package R (Lavigne and Gattuso, 2010).

α_B = isotopic fractionation factor in seawater at 25 °C is 1.0272 ± 0.0006 (Klochko et al., 2006) with precautions concerning its use for cold-water corals are given in McCulloch et al. (2012)

$\delta^{11}B_{sw}$ = boron isotope composition of seawater is 39.61 ‰ (Foster et al., 2010)

$\delta^{11}B_C$ = measured δ^{11}B of the studied coral specimen.

For SIMS measurements we used the Cameca-ims-f4 at the EMMAC facility, University of Edinburgh with the following measuring procedure: the sections were gold-

coated and analyzed with a $^{16}O_2^-$ primary beam with a primary beam energy of 15 keV and a beam current between 10 and 40 nA to produce positive secondary ions of $10B^+$ and $11B^+$. The secondary ions were analysed with an energy window of 52 eV, a 150 μm image field using 450 μm contrast and 1800 μm field apertures. The isotope ratio was measured for 200 cycles, each cycle consisting of 5 and 3 s integrations of $10B^+$ and $11B^+$ respectively. The beam diameter at the end of the analysis was ∼ 25 by 40 μm. Surface contamination was minimised using a 30 s pre-sputter, Köhler illumination with a field aperture limiting ions to the central area of the sputter pit. For details see Kasemann et al. (2009).

Analyses followed line-transects and single spots were spaced ∼ 30–50 μm apart (depending on the sampling location). A minimum of 10 spot analyses of the internal standard M93 coral bulk standard (Kasemann et al., 2009) (24.8±0.4‰ (2SD)) was run each day of analyses, with an average of 3.79 ± 0.44‰ (1SE) and used to normalize sample $^{11}B/^{10}B$ values. The internal precision for a single spot was approximately 1.0‰.

3 Results

Skeletal tomography reveals a large degree of morphological variability within the *L. pertusa* skeleton. Both the thickness of the outer wall and septa vary strongly as do the shape and length of the septa. In addition, the vertical extension of newly developed material (after staining) was not even (Fig. 1a). Therefore to enable a direct comparison between the natural material and that grown at high CO_2, sections were taken directly above and below the Alizarin stain (Fig. 1b). These sections show that there is no change in skeletal strength and structure for three different pCO_2 treatments (Fig. 1 c–h), i.e. there is no morphological sign indicating a stress response.

The main growing edge outlined by the Alizarin staining lines marks the border to the experimentally precipitated distal skeleton (see electronic Fig. Sb). In microscopic images the staining line is only visible at the main growing edge (see electronic Fig. S1b),

whereas in Raman fluorescence maps the outer skeletal surface before the start of the experiment can be traced over the entire colony (see Figs. S1, S2 in the Supplement). The Raman maps display the orientation of the skeletal fibres and the location of the early mineralization zone (EMZ: Cuif and Dauphin, 2005, or rapid accretion front, RAF Stolarski, 2003) and were used to compare skeletal formation before and during experimental conditions (see Fig. S1c, d). At the macromorphological level, i.e. the arrangement of the main skeleton entities (EMZ and fibres), no notable difference between the natural and high pCO_2 sample can be detected (Figs. 3–5b, see electronic Fig. S2b and c) and thus, elevated pCO_2 do not affect the macromorphological growth pattern. However, the organic matrix layers of the fibre growth layers between natural conditions and the high pCO_2 individual (Fig. 2c and d vs. Fig. 5d and e) were less distinct in the latter.

All the samples analysed showed heterogeneity in $\delta^{11}B$ varying from ∼ 19.8–32.2 ‰, in particular when old branches with large secondary thickening were analysed (Fig. 4a, S2). The variability of $\delta^{11}B$ in *L. pertusa* spans approx. 14 ‰ and reveals lower values within the primary skeleton around the EMZ 22.48 ± 1.58 ‰ (mean ± SD, see Table S2) and an increase towards the outer skeletal rims (Figs. 4–5, see electronic Figs. S2, S3). The secondary thickening is characterized by elevated $\delta^{11}B$ of 26.97 ± 4.73 ‰ and slightly reduced values at opaque nucleation sites (Figs. 3 and 4, see electronic Fig. S3, Table S2). The staining line showed reduced $\delta^{11}B$ values (Fig. 3, S4) and this growth period was therefore associated with reduced pH up-regulation.

Material that was deposited along the same skeletal region has the same $\delta^{11}B$ (shown by multiple transect; Figs. 4 and 5). The secondary thickening has the same $\delta^{11}B$ independent of whether it was precipitated during natural or the high pCO_2 condition (26.97 ± 4.73 and 27.8 ± 1.94 ‰, respectively; Fig. 3c). The sample grown only under high pCO_2 has slightly elevated average $\delta^{11}B$ (24.52 ± 1.21 ‰) within the primary skeleton (Fig. 6) compared to primary skeleton precipitated under natural conditions. During the formation of the primary skeleton the calculated internal calcifying

fluid pH_{cf} is lower compared to secondary thickening (8.58 ± 0.11 vs. 8.94 ± 0.15). The primary skeleton formed during high pCO_2 conditions reveals a stronger internal pH up-regulation (8.74 ± 0.08) but still lower than what was measured within the secondary thickening during high CO_2 conditions (8.95 ± 0.13).

4 Discussion

Lophelia pertusa has been shown to grow in undersaturated conditions; the amount of aragonite deposited under higher CO_2 was at least equivalent to that deposited under natural conditions (Form and Riebesell, 2012; Hennige et al., 2014; Maier et al., 2012). As *L. pertusa* grows by both vertical extension and by thickening, measurements by buoyant weight does not provide information on whether the morphology is affected, i.e. does the skeleton thicken or thin during low saturation or remain unchanged. Tomographic analyses clearly showed that the morphology of *Lophelia* skeletons are highly variable and does not change under high CO_2 even in undersaturated waters, i.e. there is no morphological indication of a stress response. We observed no change in skeletal strength and structure in contrast to what was seen in other calcifying organisms, who show wall deformation for example (Chan et al., 2012; Ragazzola et al., 2012). Arrangement and size of the primary skeleton, the template of size and shape of the corallite, does not change between treatments. The succession of growth bands is maintained and layers are formed even at undersaturated conditions. This finding corroborates Janiszewska et al. (2011) assessment of the strong biological control on deep sea Scleractinian coral biomineralisation, despite a wide range of environmental conditions. The only observed exception was the less distinct organic layers, which might represent a step compromised in biomineralisation and a potential ocean acidification impact. The wider implications of a changed skeletal organic matrix need to be investigated, in particular, the effects on the skeletal structure in future cold-water coral reefs.

A strong biological control on the biomineralisation should also be expressed in its chemical composition, especially the boron isotope compositions (McCulloch et al., 2012). For deep-water corals grown in relatively stable environmental conditions, the high-resolution spatial isotopic and elemental heterogeneities suggest a biotic control that changes during growth. The isotopic heterogeneity is associated with specific skeletal regions (Blamart et al., 2007) and is also observed in other isotopes, e.g. $\delta^{18}O$ (e.g. Rollion-Bard et al., 2010) and elemental ratios, e.g. Mg/Ca (e.g. Cohen et al., 2006). The Early Mineralization Zone (EMZ) is characterised with relatively low $\delta^{11}B$, while adjacent fibrous aragonite has a higher $\delta^{11}B$ and increases towards the outer wall. The EMZ is also known to have systematically lighter C and O isotopic composition by ~ 4–5 and ~ 8–10 ‰ respectively, compared to the fibrous aragonite part (Juillet-Leclerc et al., 2009; Rollion-Bard et al., 2010). Differences in C and O isotopes are suggested to be related to a faster growth of the EMZ. This means that different skeletal regions are potentially subjected to different control or even precipitation mechanisms. While the degree of heterogeneity with respect to boron isotopes in our samples is roughly equivalent to that of Blamart et al. (2007), the absolute values disagree with an offset of ~ 10–14 ‰. In their study the $\delta^{11}B$ translates to a maximum pH$_{cf}$ of approximately 10.2, while our data agree with the bulk measurements of *L. pertusa* (McCulloch et al., 2012) and the expected internal pH$_{cf}$ of Scleractinian corals (Al-Horani et al., 2003).

Our interpretations hence are based on the currently widely used internal pH$_{cf}$ regulation calcification model (McCulloch et al., 2012). The model assumes that the pH$_{cf}$ is offset from seawater pH$_{sw}$ (or more precisely aragonite saturation state). McCulloch et al. (2012) reported a decrease in $\delta^{11}B$ with decreasing pH$_{sw}$ in several cold-water coral species. In *L. pertusa* the relationship was only a weak relationship; however, after translating the data into ΔpH, a stronger relationship was observed. This suggested that the biological pH$_{cf}$ up-regulation determines the calcification response as described for tropical corals (Holcomb et al., 2014). The corals investigated here, however, had similar growth rates between pCO$_2$ treatments (Form and Riebesell, 2012)

and similar δ^{11}B values which contradicts anticipated decreasing internal pH$_{cf}$ (Anagnostou et al., 2012; McCulloch et al., 2012). This finding has important consequences for using *L. pertusa* as a proxy carrier for δ^{11}B studies of past oceans.

Given a sufficient food supply, calcification can be maintained despite low saturation state, as has been suggested in other corals or organisms (Schoepf et al., 2013; Thomsen et al., 2013). If food was provided in excess of normal conditions, additional energy might have been available to support calcification. If this was the case, then more food-limited conditions potentially result in a differing response to that found under laboratory conditions. Limitations in food availability might have a stronger influence than seawater pH$_{sw}$ and govern the in situ results. Respiration rates of *Lophelia* were observed to decline (Hennige et al., 2014) as well as to be unchanged (Maier et al., 2013) under elevated pCO$_2$ suggesting that other energy sources, e.g. lipids, were used to maintain growth assuming other metabolic processes remained constant. Form and Riebesell (2012) found that respiration rates declined with increasing pCO$_2$ however it was not monitored whether this results in changes in the availability of energy reserves or in tissue biomass between the treatments. Therefore, this permits to draw conclusions and understand the full consequences of a stronger pH up-regulation and associated increased energy requirements.

The secondary skeleton pH$_{cf}$ values are reasonable and corroborate cold-water coral resilience, whereas the pH$_{cf}$ regulation model fails to explain the values within the primary skeleton with an expected higher growth rate (deduced from δ^{18}O e.g. Adkins et al., 2003; Rollion-Bard et al., 2010) and hence expected higher pH$_{cf}$ values (Adkins et al., 2003). This suggests that rate-dependent pH$_{cf}$ up-regulation is potentially outruled/overridden by other prevalent conditions.

Using δ^{11}B as pH$_{sw}$ proxy is based on exclusive borate incorporation. However, NMR studies questioned this assumption by analysing ^{11}B coordination in biogenic carbonates (Klochko et al., 2009; Rollion-Bard et al., 2011). A previous study found that both borate and boric acid are incorporated in the skeleton of *Lophelia pertusa*. It has been found that boric acid was 48 % in the EMZ and 18 % in the secondary thick-

ening (Rollion-Bard et al., 2011; see electronic Fig. S5). The authors proposed that by correcting for the amount of boric acid incorporation, (a) the seawater pH can be reconstructed from the boron isotopic signature of the EMZ and (b) the secondary thickening pH_{cf} falls within the range measured by microsensors (Al-Horani, 2003; Ries, 2011).

5 In contrast, here the $\delta^{11}B$ in the secondary thickening parts already reflects the expected pH_{cf} (see Fig. S5). Moreover, our data do not allow the proposed seawater pH reconstruction from the EMZ $\delta^{11}B$ when we used their measured boric acid content. Thus, either no boric acid is incorporated or the proportion is not species specific and depends on the individual. The latter would complicate any reconstruction of seawater

10 conditions when the individual has such a strong control over the element incorporation.

In biomineralisation research, skeletal organic matrix and amorphous calcium carbonate (ACC) can play crucial roles. Although ACC plays a major role in biomineralisation in various calcifying organisms (Addadi et al., 2006; Falini et al., 2013; Goffredo

15 et al., 2011), it has not yet been described as a precursor for coral calcification though it cannot be unequivocally discounted (Clode et al., 2010). If ACC also represents a first step in coral calcification, there is no indication how this amorphous crystalline transition affects isotopic fractionation and whether it can account for the observed isotopic offsets between primary skeleton and secondary thickening. We have found indications

20 of changes in the organic matrix (OM). The less distinct OM bands could be an important step compromised in biomineralisation under ocean acidification. It was shown that OM production can be affected in a tropical coral with both up and down regulation of certain OM protein encoding genes (Moya et al., 2012), which might affect the quality of the OM. In addition, the increased energy demand for up-regulation could further

25 restrict the OM production and coral biomineralisation over longer time scales.

In conclusion, the lack of sensitivity of *L. pertusa* to changes in pCO$_2$ corroborates their strong biological control over biomineralisation that is not easily disturbed under elevated pCO$_2$ conditions in well-fed corals. Our results have important implications for the use of $\delta^{11}B$ as a pH proxy and for studying coral biomineralisation: (1) addi-

tional energy might potentially be utilised to up-regulate the internal pH_{cf} to a suitable level which would then complicate or even negate the utility of *Lophelia skeletons* δ^{11}B record as a paleo-pH proxy, (2) the additional energy needed to support the biomineralisation does not necessarily compromise its structure and (3) both spatial heterogene-

5 ity of δ^{11}B within the sample as well as the role of OM production and quality need to be considered to improve our understanding of cold-water coral biomineralisation and their response to acidification.

The Supplement related to this article is available online at doi:10.5194/bgd-12-6757-2015-supplement.

Full Screen / Esc

Printer-friendly Version

Interactive Discussion

References

Addadi, L., Joester, D., Nudelman, F., and Weiner, S.: Mollusk shell formation: a source of new concepts for understanding biomineralization processes, Chemistry, 12, 980–987, doi:10.1002/chem.200500980, 2006.

Adkins, J. F., Boyle, E. A., Curry, W. B., and Lutringer, A.: Stable isotopes in deep-sea corals and a new mechanism for "vital effects", Geochim. Cosmochim. Ac., 67, 1129–1143, doi:10.1016/S0016-7037(02)01203-6, 2003.

Al-Horani, F.: Microsensor study of photosynthesis and calcification in the scleractinian coral, Galaxea fascicularis: active internal carbon cycle, J. Exp. Mar. Biol. Ecol., 288, 1–15, doi:10.1016/S0022-0981(02)00578-6, 2003.

Al-Horani, F. A., Al-Moghrabi, S. M., and de Beer, D.: The mechanism of calcification and its relation to photosynthesis and respiration in the scleractinian coral *Galaxea fascicularis*, Mar. Biol., 142, 419–426, doi:10.1007/s00227-002-0981-8, 2003.

Anagnostou, E., Huang, K., You, C., Sikes, E. L., and Sherrell, R. M.: Evaluation of boron isotope ratio as a pH proxy in the deep sea coral *Desmophyllum dianthus*: evidence of physiological pH adjustment, Earth Planet. Sc. Lett., 349–350, 251–260, doi:10.1016/j.epsl.2012.07.006, 2012.

Bates, N. R., Best, M. H. P., Neely, K., Garley, R., Dickson, A. G., and Johnson, R. J.: Detecting anthropogenic carbon dioxide uptake and ocean acidification in the North Atlantic Ocean, Biogeosciences, 9, 2509–2522, doi:10.5194/bg-9-2509-2012, 2012.

Blamart, D., Rollion-Bard, C., Meibom, A., Cuif, J.-P., Juillet-Leclerc, A., and Dauphin, Y.: Correlation of boron isotopic composition with ultrastructure in the deep-sea coral *Lophelia pertusa*: implications for biomineralization and paleo-pH, Geochem. Geophy. Geosy., 8, 1–11, doi:10.1029/2007GC001686, 2007.

Chalker, B. E. and Taylor, D. L.: Light-enhanced calcification, and the role of oxidative phosphorylation in calcification of the coral Acropora cervicornis, P. Roy. Soc. B.-Biol. Sci., 190, 323–331, 1975.

Chan, V. B. S., Li, C., Lane, A. C., Wang, Y., Lu, X., Shih, K., Zhang, T., and Thiyagarajan, V.: $CO_{(2)}$-driven ocean acidification alters and weakens integrity of the calcareous tubes produced by the serpulid tubeworm, *Hydroides elegans.*, PLoS One, 7, e42718, doi:10.1371/journal.pone.0042718, 2012.

Clode, P. L., Lema, K., Saunders, M., and Weiner, S.: Skeletal mineralogy of newly settling *Acropora millepora* (Scleractinia) coral recruits, Coral Reefs, 30, 1–8, doi:10.1007/s00338-010-0673-7, 2010.

Cohen, A. L., Gaetani, G. A., Lundälv, T., Corliss, B. H., and George, R. Y.: Compositional variability in a cold-water scleractinian, *Lophelia pertusa*: new insights into "vital effects", Geochem. Geophy. Geosy., 7, Q12004, doi:10.1029/2006GC001354, 2006.

Cuif, J. P. and Dauphin, Y.: The two-step mode of growth in the scleractinian coral skeletons from the micrometre to the overall scale, J. Struct. Biol., 150, 319–331, doi:10.1016/j.jsb.2005.03.004, 2005.

Davies, A. J. and Guinotte, J. M.: Global habitat suitability for framework-forming cold-water corals., PLoS One, 6, e18483, doi:10.1371/journal.pone.0018483, 2011.

Dickson, A. G.: Standard potential of the reaction: AgCl(s) +1/2H$_2$(g) = Ag(s) + HCl(aq) and the standard acidity constant of the ion HSO$_4^-$ in synthetic seawater from 273/15 to 318.15 K, J. Chem. Thermodyn., 22, 113–127, 1990.

Doney, S. C., Fabry, V. J., Feely, R. A., and Kleypas, J. A.: Ocean acidification: the other CO_2 problem, Ann. Rev. Mar. Sci., 1, 169–192, doi:10.1146/annurev.marine.010908.163834, 2009.

Falini, G., Reggi, M., Fermani, S., Sparla, F., Goffredo, S., Dubinsky, Z., Levi, O., Dauphin, Y., and Cuif, J. P.: Control of aragonite deposition in colonial corals by intra-skeletal macro-molecules., J. Struct. Biol., 183, 226–38, doi:10.1016/j.jsb.2013.05.001, 2013.

Feely, R. A., Sabine, C. L., Lee, K., Berelson, W., Kleypas, J., Fabry, V. J., and Millero, F. J.: Impact of anthropogenic CO_2 on the $CaCO_3$ system in the oceans, Science, 305, 362–6, doi:10.1126/science.1097329, 2004.

Form, A. U. and Riebesell, U.: Acclimation to ocean acidification during long-term CO_2 exposure in the cold-water coral *Lophelia pertusa*, Glob. Change Biol., 18, 843–853, doi:10.1111/j.1365-2486.2011.02583.x, 2012.

Fosså, J. H., Mortensen, P. B., and Furevik, D. M.: The deep-water coral *Lophelia pertusa* in Norwegian waters: distribution and fishery impacts, Hydrobiologia, 471, 1–12, 2002.

Foster, G. L., Pogge von Strandmann, P. A. E., and Rae, J. W. B.: Boron and magnesium isotopic composition of seawater, Geochem. Geophy. Geosy., 11, Q08015, doi:10.1029/2010GC003201, 2010.

Genin, A., Dayton, P. K., Lonsdale, P. F., and Spiess, F. N.: Corals on seamount peaks provide evidence of current acceleration over deep-sea topography, Nature, 322, 59–61, 1986.

Goffredo, S., Vergni, P., Reggi, M., Caroselli, E., Sparla, F., Levy, O., Dubinsky, Z., and Falini, G.: The skeletal organic matrix from Mediterranean coral *Balanophyllia europaea* influences calcium carbonate precipitation, PLoS One, 6, e22338, doi:10.1371/journal.pone.0022338, 2011.

Guinotte, J. M. and Fabry, V. J.: Ocean acidification and its potential effects on marine ecosystems, Ann. NY Acad. Sci., 1134, 320–42, doi:10.1196/annals.1439.013, 2008.

Hennige, S. J., Wicks, L. C., Kamenos, N. a., Bakker, D. C. E., Findlay, H. S., Dumousseaud, C., and Roberts, J. M.: Short-term metabolic and growth responses of the cold-water coral *Lophelia pertusa* to ocean acidification, Deep Sea Res. Part II Top. Stud. Oceanogr., 99, 27–35, doi:10.1016/j.dsr2.2013.07.005, 2014.

Henry, L. A. and Roberts, J. M.: Biodiversity and ecological composition of macrobenthos on cold-water coral mounds and adjacent off-mound habitat in the bathyal Porcupine Seabight, NE Atlantic, Deep Sea Res. Part I Oceanogr. Res. Pap., 54, 654–672, doi:10.1016/j.dsr.2007.01.005, 2007.

Holcomb, M., Venn, A. A., Tambutté, E., Tambutté, S., Allemand, D., Trotter, J., and McCulloch, M.: Coral calcifying fluid pH dictates response to ocean acidification., Sci. Rep., 4, 5207, doi:10.1038/srep05207, 2014.

Janiszewska, K., Stolarski, J., Benzerara, K., Meibom, A., Mazur, M., Kitahara, M. V. and Cairns, S. D.: A unique skeletal microstructure of the deep-sea micrabaciid scleractinian corals., J. Morphol., 272, 191–203, doi:10.1002/jmor.10906, 2011.

Juillet-Leclerc, A., Reynaud, S., Rollion-Bard, C., Cuif, J. P., Dauphin, Y., Blamart, D., Ferrier-Pagès, C., and Allemand, D.: Oxygen isotopic signature of the skeletal microstructures in cultured corals: identification of vital effects, Geochim. Cosmochim. Ac., 73, 5320–5332, doi:10.1016/j.gca.2009.05.068, 2009.

Kasemann, S. A., Schmidt, D. N., Bijma, J., and Foster, G. L.: In situ boron isotope analysis in marine carbonates and its application for foraminifera and palaeo-pH, Chem. Geol., 260, 138–147, doi:10.1016/j.chemgeo.2008.12.015, 2009.

Klochko, K., Kaufman, A. J., Yao, W., Byrne, R. H., and Tossell, J. A.: Experimental measurement of boron isotope fractionation in seawater, Earth Planet. Sc. Lett., 248, 276–285, doi:10.1016/j.epsl.2006.05.034, 2006.

Klochko, K., Cody, G. D., Tossell, J. A., Dera, P., and Kaufman, A. J.: Re-evaluating boron speciation in biogenic calcite and aragonite using 11B MAS NMR, Geochim. Cosmochim. Ac., 73, 1890–1900, doi:10.1016/j.gca.2009.01.002, 2009.

Lavigne, H. and Gattuso, J.: seacarb: seawater carbonate chemistry with R package version 3.0., 2010.

Maier, C., Bils, F., Weinbauer, M. G., Watremez, P., Peck, M. A., and Gattuso, J. P.: Respiration of Mediterranean cold-water corals is not affected by ocean acidification as projected for the end of the century, Biogeosciences, 10, 5671–5680, doi:10.5194/bg-10-5671-2013, 2013.

Maier, C., Hegeman, J., Weinbauer, M. G., and Gattuso, J.-P.: Calcification of the cold-water coral *Lophelia pertusa*, under ambient and reduced pH, Biogeosciences, 6, 1671–1680, doi:10.5194/bg-6-1671-2009, 2009.

Maier, C., Watremez, P., Taviani, M., Weinbauer, M. G., and Gattuso, J. P.: Calcification rates and the effect of ocean acidification on Mediterranean cold-water corals., P. Roy. Soc. B.-Biol. Sci., 279, 1716–23, doi:10.1098/rspb.2011.1763, 2012.

McCulloch, M., Trotter, J., Montagna, P., Falter, J., Dunbar, R., Freiwald, A., Försterra, G., López Correa, M., Maier, C., Rüggeberg, A., and Taviani, M.: Resilience of cold-water scleractinian corals to ocean acidification: boron isotopic systematics of pH and saturation state up-regulation, Geochim. Cosmochim. Ac., 87, 21–34, doi:10.1016/j.gca.2012.03.027, 2012.

Mienis, F., De Stigter, H. C., White, M., Duineveld, G., De Haas, H., and Van Weering, T. C. E.: Hydrodynamic controls on cold-water coral growth and carbonate-mound development at the SW and SE Rockall Trough Margin, NE Atlantic Ocean, Deep Sea Res. Part I Oceanogr. Res. Pap., 54, 1655–1674, 2007.

Mortensen, P. B. and Rapp, H. T.: Oxygen and carbon isotope ratios related to growth line patterns in skeletons of *Lophelia pertusa* (L) (Anthozoa, Scleractinia): implicaitons for determination of linear extension rates, Sarsia, 83, 433–446, 1998.

Moya, A, Huisman, L., Ball, E. E., Hayward, D. C., Grasso, L. C., Chua, C. M., Woo, H. N., Gattuso, J. P., Forêt, S., and Miller, D. J.: Whole transcriptome analysis of the coral *Acropora millepora* reveals complex responses to CO_2-driven acidification during the initiation of calcification., Mol. Ecol., 21, 2440–54, doi:10.1111/j.1365-294X.2012.05554.x, 2012.

Orr, J. C., Fabry, V. J., Aumont, O., Bopp, L., Doney, S. C., Feely, R. A, Gnanadesikan, A., Gru-
ber, N., Ishida, A., Joos, F., Key, R. M., Lindsay, K., Maier-Reimer, E., Matear, R., Monfray, P.,
Mouchet, A., Najjar, R. G., Plattner, G. K., Rodgers, K. B., Sabine, C. L., Sarmiento, J. L.,
Schlitzer, R., Slater, R. D., Totterdell, I. J., Weirig, M. F., Yamanaka, Y., and Yool, A.: Anthro-
pogenic ocean acidification over the twenty-first century and its impact on calcifying organ-
isms., Nature, 437, 681–6, doi:10.1038/nature04095, 2005a.

Orr, J. C., Fabry, V. J., Aumont, O., Bopp, L., Doney, S. C., Feely, R. A., Gnanadesikan, A.,
Gruber, N., Ishida, A., Joos, F., Key, R. M., Lindsay, K., Maier-reimer, E., Matear, R., Mon-
fray, P., Mouchet, A., Najjar, R. G., Slater, R. D., Totterdell, I. J., Weirig, M., Yamanaka, Y.,
and Yool, A.: Anthropogenic ocean acidification over the twenty-first century and its impact
on calcifying organisms, Nature, 437, 681–686, doi:10.1038/nature04095, 2005b.

Ragazzola, F., Foster, L. C., Form, A., Anderson, P. S. L., Hansteen, T. H., and Fietzke, J.:
Ocean acidification weakens the structural integrity of coralline algae, Glob. Change Biol.,
18, 2804–2812, doi:10.1111/j.1365-2486.2012.02756.x, 2012.

Ries, J. B.: A physicochemical framework for interpreting the biological calcification re-
sponse to CO_2-induced ocean acidification, Geochim. Cosmochim. Ac., 75, 4053–4064,
doi:10.1016/j.gca.2011.04.025, 2011.

Ries, J. B., Cohen, A. L., and McCorkle, D. C.: Marine calcifiers exhibit mixed responses to
CO_2-induced ocean acidification, Geology, 37, 1131–1134, doi:10.1130/G30210A.1, 2009.

Roberts, M., Henry, L. A., Long, D., and Hartley, J. P.: Cold-water coral reef frameworks and en-
hanced megafaunal diversity on the Hatton Bank, NE Atlantic, Facies, 54, 1297–316, 2008.

Rollion-Bard, C., Blamart, D., Cuif, J. P., and Dauphin, Y.: In situ measurements of oxy-
gen isotopic composition in deep-sea coral, *Lophelia pertusa*: re-examination of the cur-
rent geochemical models of biomineralization, Geochim. Cosmochim. Ac., 74, 1338–1349,
doi:10.1016/j.gca.2009.11.011, 2010.

Rollion-Bard, C., Blamart, D., Trebosc, J., Tricot, G., Mussi, A., and Cuif, J. P.: Boron isotopes
as pH proxy?: a new look at boron speciation in deep-sea corals using 11 B MAS NMR and
EELS, Geochim. Cosmochim. Ac., 75, 1003–1012, doi:10.1016/j.gca.2010.11.023, 2011.

Schoepf, V., Grottoli, A. G., Warner, M. E., Cai, W. J., Melman, T. F., Hoadley, K. D., Pet-
tay, D. T., Hu, X., Li, Q., Xu, H., Wang, Y., Matsui, Y., and Baumann, J. H.: Coral energy
reserves and calcification in a high-CO_2 world at two temperatures., PLoS One, 8, e75049,
doi:10.1371/journal.pone.0075049, 2013.

Stampanoni, M., Groso, A., Isenegger, A., Mikuljan, G., Chen, Q., Bertrand, A., Henein, S., Betemps, R., Frommherz, U., Böhler, P., Meister, D., Lange, M., Abela, R., and Boehler, P.: Trends in synchrotron-based tomographic imaging: the SLS experience, Dev. X-Ray Tomogr. V, 6318, doi:10.1117/12.679497, 2006.

5 Stolarski, J.: Three – dimensional micro – and nanostructural characteristics of the scleractinian coral skeleton: a biocalcification proxy, Acta Palaeontol. Pol., 48, 497–530, 2003.

Thomsen, J., Casties, I., Pansch, C., Körtzinger, A., and Melzner, F.: Food availability outweighs ocean acidification effects in juvenile *Mytilus edulis*: laboratory and field experiments., Glob. Change Biol., 19, 1017–27, doi:10.1111/gcb.12109, 2013.

10 Trotter, J., Montagna, P., McCulloch, M., Silenzi, S., Reynaud, S., Mortimer, G., Martin, S., Ferrier-Pagès, C., Gattuso, J. P., and Rodolfo-Metalpa, R.: Quantifying the pH "vital effect" in the temperate zooxanthellate coral *Cladocora caespitosa*: validation of the boron seawater pH proxy, Earth Planet. Sc. Lett., 303, 163–173, doi:10.1016/j.epsl.2011.01.030, 2011.

Venn, A. A., Tambutté, E., Holcomb, M., Laurent, J., Allemand, D., and Tambutté, S.: Impact of
15 seawater acidification on pH at the tissue – skeleton interface and calcification in reef corals, P. Natl. Acad. Sci. USA, 110, 1634–1639, doi:10.1073/pnas.1216153110, 2013.

Wainright, S. A.: Studies of the mineral phase of coral skeleton, Exp. Cell Res., 34, 213–230, 1964.

Wall, M. and Nehrke, G.: Reconstructing skeletal fiber arrangement and growth mode in the
20 coral *Porites lutea* (Cnidaria, Scleractinia): a confocal Raman microscopy study, Biogeosciences, 9, 4885–4895, doi:10.5194/bg-9-4885-2012, 2012.
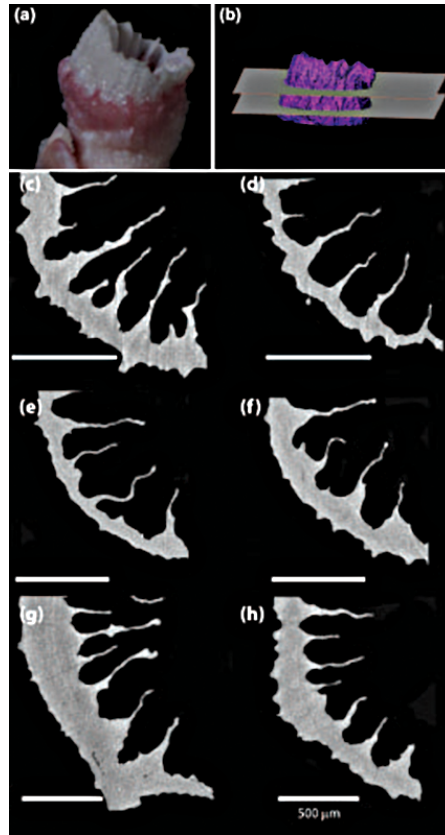
Figure 1. (a) Polyp with Alizarin stain and **(b)** reconstructed SRXTM 3-D virtual model. This comparison allowed the virtual polyp to be sectioned below (left panel) and above (right panel) the Alizarin stain. Virtual SXRTM cross-sections of polyps for different $p\text{CO}_2$ treatment 604 µatm **(c, d)**, 778 µatm **(e, f)** and 982 µatm **(g, h)**.
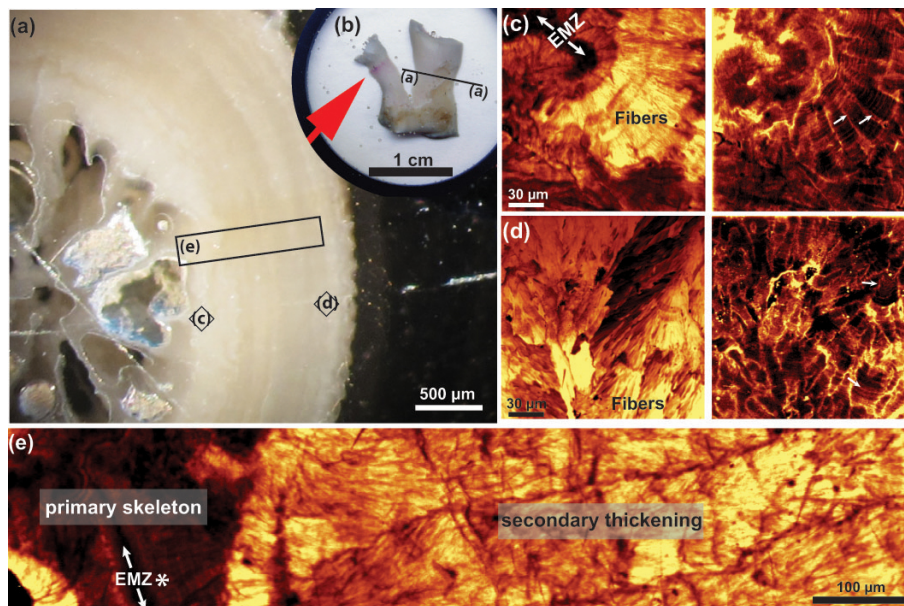
Figure 2. *Lophelia pertusa* colony **(a)** cut in transversal plane of an old branch and **(b)** *Lophelia* colony cut in longitudinal plane with two branches (old and a young branch). The young side branch shows the Alizarin stain. **(c, d)** Raman maps of aragonite fibre orientation (left map) and fluorescence (right map) within the primary skeleton with early mineralization zone (EMZ; **(c)** and within the secondary thickening **(d)**. The arrows in **(c, d)** mark skeletal organic matrix bands. **(e)** Raman maps of aragonite fibre orientation clearly differentiating primary skeleton and secondary thickening of the corallite and early mineralization zone (EMZ).
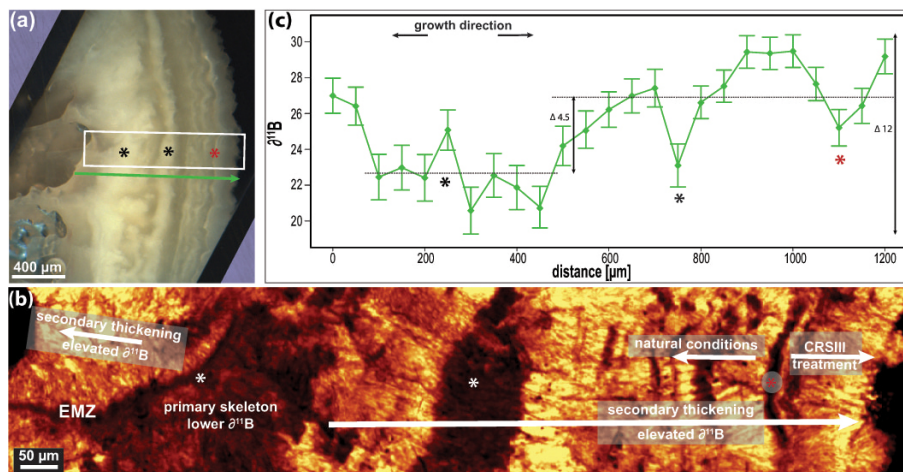
Figure 3. Old branch of *Lophelia pertusa* cut in transversal plane and prepared for Raman mapping and SIMS analysis. **(a)** Microscopic image of transversal cut through an old branch displaying the location of the Raman map and SIMS transect. **(b)** Raman map of the intensity distribution of the main aragonite peak (symmetric stretch, $1085\,cm^{-1}$) reveals the early mineralization zone (EMZ), the primary skeleton and the area of secondary thickening. Asterisks mark EMZ in the primary skeleton and skeletal areas within the secondary thickening zone of potentially reduced Boron isotopic value (cf. opaque growth bands in Blamart et al., 2007 or 1°, 2° nucleation zone in Cohen et al., 2006). Red asterisk marks the location of the staining line and hence, the border between growth under natural/control condition and laboratory treatment. **(c)** $\delta^{11}B$ measured in growth direction from inside to the outer coral skeletal rim (transect #1).

Full Screen / Esc

Printer-friendly Version

Interactive Discussion
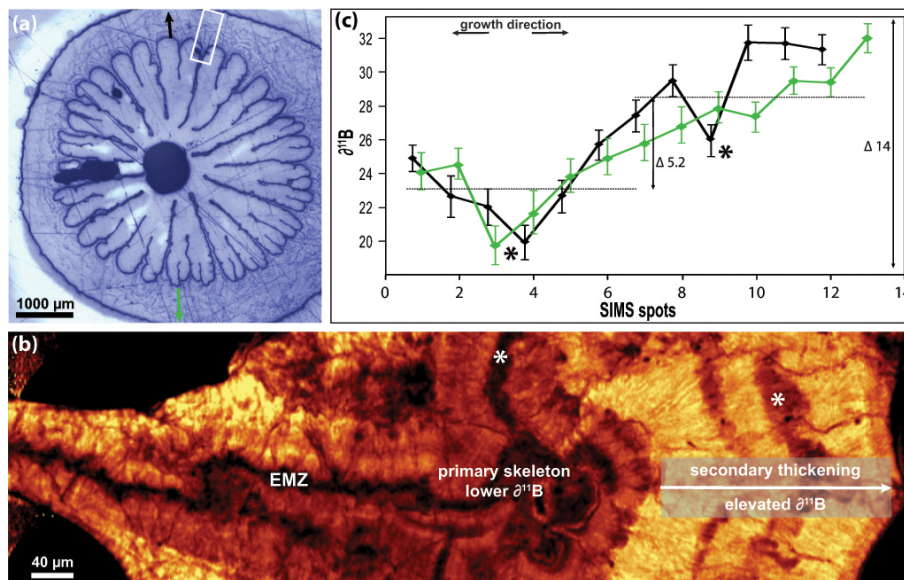
Figure 4. Side branch of *Lophelia pertusa* cut in transversal plane and prepared for Raman mapping and SIMS analysis. **(a)** Microscopic image contains the location of the Raman map and the SIMS transects. **(b)** Raman map of the intensity distribution of the main aragonite peak (symmetric stretch, $1085\,cm^{-1}$) reveals the early mineralization zone (EMZ), the primary skeleton and the area of secondary thickening. Asterisks mark EMZ in the primary skeleton and skeletal areas within the secondary thickening zone of potentially reduced Boron isotopic value (cf. opaque growth bands in Blamart et al., 2007 or 1°, 2° nucleation zone in Cohen et al., 2006). **(c)** δ^{11}B measured from inside to the outer coral skeletal rims (transect #2,3).
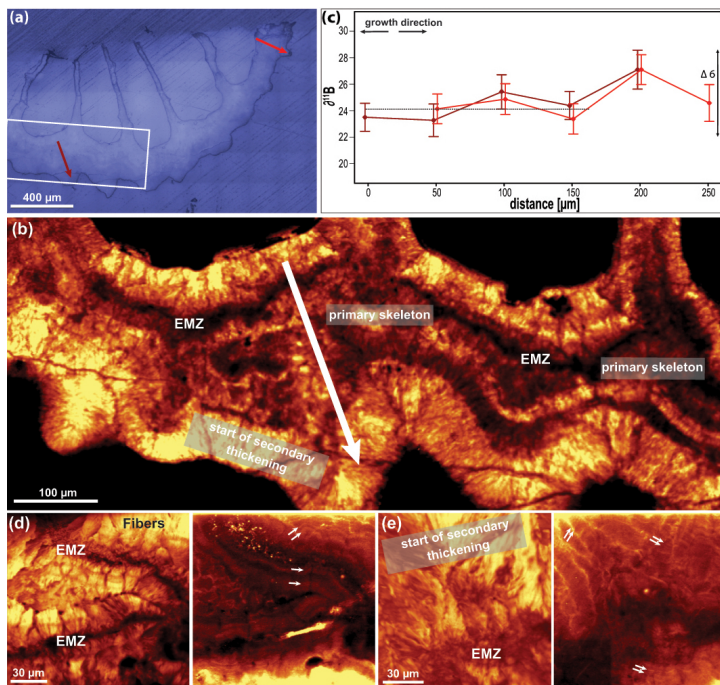
Figure 5. New branch of *Lophelia pertusa* cut above the staining line in transversal plane and prepared for Raman mapping and SIMS analysis. **(a)** Microscopic image displays the location of the Raman map and the SIMS transects. **(b)** Raman map of the intensity distribution of the main aragonite peak (symmetric stretch, $1085\,\text{cm}^{-1}$) reveals the early mineralization zone (EMZ), the primary skeleton and the start of secondary thickening. **(c)** $\delta^{11}B$ measured from inside to the outer coral skeletal rim (transect #4,5). **(d, e)** Raman maps of aragonite fibre orientation (left map) and fluorescence (right map) within the primary skeleton with early mineralization zone (EMZ) and with starting of the secondary thickening **(e)**. The arrows in **(d, e)** mark skeletal organic matrix bands.